Nanoscale

Halide-Assisted Metal Ion Reduction: Emergent Effects of Dilute Chloride, Bromide, and Iodide in Nanoparticle Synthesis

Journal:	*Nanoscale*
Manuscript ID	NR-ART-05-2019-004647.R1
Article Type:	Paper
Date Submitted by the Author:	26-Jul-2019
Complete List of Authors:	King, Melissa; Wesleyan University, Chemistry Kent, Isabella; Wesleyan University, Chemistry Personick, Michelle; Wesleyan University, Chemistry

Halide-Assisted Metal Ion Reduction: Emergent Effects of Dilute Chloride, Bromide, and Iodide in Nanoparticle Synthesis

Melissa E. King, Isabella A. Kent, and Michelle L. Personick*

Department of Chemistry, Wesleyan University, Middletown, Connecticut 06459, United States

*Email: mpersonick@wesleyan.edu

Abstract

Understanding the competing effects of growth-directing additives, such as halide ions, on particle formation in solution phase metal nanoparticle syntheses is an ongoing challenge. Further, trace halide impurities are known to have a drastic impact on particle morphology as well as reproducibility. Herein, we employ a "halide-free" platform as an analogue to commonly used halide-containing surfactants and metal precursors to isolate and study the effects of micromolar concentrations of halide ions (chloride, bromide, and iodide) on the rate of metal ion reduction. In the absence of competing halides from precursors and surfactants, we observe a catalytic effect of low concentrations of halide ions on the rate of metal ion reduction, an influence which is fundamentally different from the previously reported role of halides in metal nanoparticle growth. We propose that this halide-assisted metal ion reduction proceeds via the formation of a halide bridge which facilitates the adsorption of the metal precursor to a growing nanoparticle and, subsequently, electron transfer from the particle surface. We then demonstrate that this process is operative not only in the well-controlled "halide-free" platform, but also in syntheses involving high concentrations of halide-containing surfactants as well as metal precursors with halide ligands. Importantly, this study shows that halide-assisted metal ion reduction can be extended to bimetallic systems and provides a handle for the directed differential control of metal ion reduction in one-pot co-reduction syntheses.

Introduction

The field of noble metal nanoparticle synthesis is constantly expanding due to the broad range of applications for these materials in optics, electronics, therapeutics, and catalysis.[1-3] The intrinsic properties of metal nanostructures can be related to size, shape, composition, or some combination thereof. For example, it has been shown that catalytic conversions can take place more selectively at specific facets[4-6] or with the introduction of a secondary metal that modifies reactivity.[7-9] Likewise, the underlying shape of a nanoparticle can dictate self-assembly to larger architectures with emergent properties.[10, 11] Indeed, much research has been done on the synthesis of such nanoparticles and has provided a library of low- and high-index faceted shapes with varying degrees of control over multi-metallic composition.[12] However, the deliberate design of these particles with respect to facet structure, homogeneity, and compositional control is still an ongoing challenge in solution phase colloidal synthesis, particularly for nanoparticles composed of two or more metals with dissimilar material and/or chemical properties.[13]

The introduction of additives to the nanoparticle growth solution has provided effective methods of influencing particle growth through selective surface passivation and kinetic effects.[14] These additives are typically in the form of small molecules or ions, and a wide variety of these species have been shown to effectively drive the shape-controlled synthesis of noble metal nanoparticles. In particular, halide ions present in aqueous phase syntheses have significant kinetic and surface passivating impacts on particle growth.[14-22] There are many examples of the use of halides to control nanoparticle shape, and a straightforward but well-known example is the synthesis of concave or convex cubes (tetrahexahedra) by simply switching from a cetyltrimethylammonium chloride (CTAC) surfactant to cetyltrimethylammonium bromide (CTAB).[23, 24] Further, the addition of secondary halides to growth systems has been shown to

dictate facet structure and composition.[25-27] For example, the incorporation of low concentrations of sodium bromide allows for the evolution of gold nanoparticles from cubes to trisoctahedra to rhombic dodecahedra.[28] This phenomenon has been attributed to selective surface passivation and affinity for the surface in the following order: $Cl^- < Br^- < I^-$, where greater affinity has been shown to slow the rate of metal ion reduction more significantly.[29] Likewise, metal ion complexes with bromide ligands have lower reduction potentials than metal precursors with chloride ligands, making them harder to reduce and slowing nanoparticle growth.

Recently, we have shown that low micromolar concentrations of iodide ions can be used to differentially control the relative rates of reduction of two metal precursors in a bimetallic system. In the combinations of metals that we have probed so far, these low concentrations of iodide increase the rate of palladium ion reduction.[19, 30] This behavior differs significantly from what has been previously reported by others for slightly higher concentrations of iodide ions, where the introduction of iodide leads to a decrease in reduction rate, passivation of {111} surfaces, or uncontrolled stellation in particle formation.[16, 17, 29] Using iodide as a selective rate-enhancing tool, we have synthesized tetradecapod-shaped particles (gold and palladium)[19] as well as cubic particles with terraced surfaces (palladium and copper).[30] In the second case, iodide plays an important role in overcoming a key challenge in the synthesis of bimetallic nanoparticles—the controlled reduction of metal precursors with different redox chemistry.

To explore the full scope of this approach beyond iodide and to better understand the emergent reduction rate enhancing effects of halides at low micromolar concentrations, we have studied the influence of low concentrations of chloride and bromide in a growth system free of inherent halide ions. These studies show that the addition of halides—chloride, bromide, or iodide—has a concentration-dependent impact on the rate of metal ion reduction that is enhancing

at low concentrations of halide and slowing at higher concentrations. In addition, the current work points to a mechanism of reduction rate modification that is fundamentally distinct from the behavior of halides in nanoparticle synthesis outside of the micromolar range. We also show that these insights can be used to explain the underlying chemistry behind previously reported observations in a gold-silver bimetallic system, which suggests that this methodology can be extended to a range of bimetallic systems as a means of controlling metal ion reduction rates in sequential co-reduction syntheses.

Experimental

Chemicals

Hexadecyltrimethylammonium hydrogen sulfate (CTA^+-HSO_4^-, > 98%) was purchased from TCI Chemicals. Cetyltrimethylammonium chloride solution (CTAC, 25 wt. % in H_2O, lot no. STBG7166 and STBH2336), L-ascorbic acid (ACS reagent, ≥ 99%), palladium nitrate hydrate ($Pd(NO_3)_2$, 99.8% (metal basis), Pd 39% min), sodium azide (NaN_3, ReagentPlus®, ≥ 99.5%), silver nitrate ($AgNO_3$, 99.9999% (trace metals basis)), and sodium borohydride ($NaBH_4$, granular, 99.99%) were purchased from Sigma-Aldrich. Tetrachlorauric acid trihydrate ($HAuCl_4 \cdot 3H_2O$, ACS, 99.99% (metals basis), Au 49.0% min), sodium chloride (NaCl, 99.99% (metal basis)), and sodium bromide (NaBr, 99.99% (metal basis)) were purchased from Alfa Aesar. Sodium thiocyanate (NaSCN, 98+%, ACS Reagent) was purchased from ACROS. Bis(p-sulfonatophenyl)phenylphosphine dihydrate dipotassium salt (BSPP, $C_6H_5P(C_6H_4SO_3K)_2 \cdot 2H_2O$, min. 97%) was purchased from STREM. Hydrochloric acid (HCl, TraceMetal™ Grade), nitric acid (HNO_3, TraceMetal™ Grade), sodium iodide (NaI, Fisher Bioreagents, ≥ 99%) were purchased from Fisher Scientific. All chemicals were used without further purification and all solutions were prepared with deionized (DI) water (18.2 MΩ resistivity, Labconco Water Pro PS).

Nanoparticle Synthesis and Kinetic Experiments

Palladium Nanoparticles in a Halide-Free Surfactant

In a typical reaction, 0.250 mL of 10 mM $Pd(NO_3)_2$ was added to 5.0 mL of 100 mM CTA^+-HSO_4^- in a 20 mL scintillation vial, followed by the addition varying concentrations of NaX (X = Cl^-, Br^-, I^-, N_3^-, or SCN^-) (Table S1). Finally, 0.05 mL of 100 mM ascorbic acid was added to initiate the reaction. Each reaction was then quenched at distinct time points over a one hour time period with 0.05 mL of 55 mM BSPP followed by vortexing to ensure rapid and uniform dispersion of BSPP.

Gold Seed Synthesis

In a typical synthesis, 0.250 mL of 10 mM $HAuCl_4$ and 0.02 mL of 1 M HCl were added to 10.0 mL of 100 mM CTAC with vigorous stirring yielding a light yellow solution. 0.60 mL of freshly prepared 10 mM $NaBH_4$ was then rapidly injected into the vigorously stirring solution to produce an orange-brown seed solution and was allowed to stir for an additional minute to ensure uniform dispersion of the reducing agent. The stirring was then halted and the seed solution was allowed to sit at room temperature for two hours.

Silver-Assisted Synthesis of Gold Nanoparticles with Added Halide

Synthesis of the gold-silver particles followed the aging of the seed reaction. To 10.0 mL of 100 mM CTAC were added 0.20 mL of 1 M HCl; 0.50 mL of 10 mM $HAuCl_4$; 40 or 100 µL of 10 mM $AgNO_3$; and either NaBr (10 mM) or NaI (1 mM) in 0, 25, or 50 µL aliquots, with gentle swirling to mix after each addition (Table S2). 0.10 mL of 100 mM ascorbic acid was then added, resulting in a color change from a light yellow solution to a clear solution. A 0.10 mL aliquot of 1000x diluted seeds (diluted in 100 mM CTAC) was then added to initiate particle growth.

Reactions were quenched at predetermined times with 0.10 mL of 65 mM BSPP followed by vortexing to ensure rapid and uniform dispersion of BSPP.

Instrumental Analysis

Inductively coupled plasma mass spectrometry (ICP-MS) analysis was carried out using a Perkin Elmer ICP-MS Elan DRC-e. Individual identical reaction solutions were used for each time point and 1.0 mL aliquots were taken from each quenched reaction vial and then centrifuged at 14,000 rpm for 15 minutes. The supernatant was removed with care to ensure the particles at the bottom of the tube were undisturbed. The particles were then washed with DI water and the previous procedure was repeated. After washing, the particles were resuspended in 1.0 mL of DI water which was then transferred to a 15 mL conical tube and digested with 2.0 mL of aqua regia (1:3 nitric acid to hydrochloric acid, CAUTION: strong acid) made from concentrated trace metal acids. The particles were allowed to digest for several hours and were then carefully diluted to 10.0 mL with DI water.

Scanning electron microscopy (SEM) images were acquired using Hitachi SU-70 and Hitachi SU-5000 field emission electron microscopes. Transmission electron microscopy (TEM) images were acquired using a FEI Tecnai Osiris 200kV TEM. Samples were prepared for SEM and TEM imaging by centrifuging a 1 mL aliquot of the reaction solution for four minutes at 6000 RPM, removing the supernatant, resuspending the particles in 1 mL of DI water, centrifuging the particles again, removing the supernatant a second time, and finally resuspending the particles in < 100 μL of DI water. A 2 μL aliquot of the washed particles was then dropcast onto a slice of silicon wafer (for SEM) or a Formvar/carbon grid (for TEM), allowed to dry, and imaged.

Speciation Calculations

Speciation calculations were performed with Hyperquad Simulation and Speciation (HySS) software[31] to estimate the solution phase palladium species using reported formation constants for chloride, bromide, iodide, and thiocyanate complexes of palladium.[32-34]

Results and Discussion

The relative reduction rates of palladium ions were probed in a cetyltrimethylammonium hydrogen sulfate (CTA^+-HSO_4^-) based growth solution with a palladium nitrate ($Pd(NO_3)_2$) precursor to remove the convoluting competition of halides that are commonly present in the starting materials (surfactants and/or metal salts). CTA^+-HSO_4^- was selected as the halide-free surfactant because it is readily commercially available. In a typical synthesis, freshly prepared $Pd(NO_3)_2$ (0.25 mL, 10 mM), and sodium chloride (NaCl), sodium bromide (NaBr), or sodium iodide (NaI) were added to CTA^+-HSO_4^- (5 mL, 100 mM). The reactions were then initiated via the addition of ascorbic acid (0.05 mL, 100 mM) at room temperature. Upon addition of the ascorbic acid reducing agent, homogeneous nucleation of seeds occurred and therefore no preformed seeds were added. These growth solutions all have a pH of approximately 1.5, which is comparable to the pH of many reported nanoparticle syntheses in more common bromide- and chloride-containing surfactants. To assess growth rates, the reactions were stopped at specific intervals over a one hour period through the introduction of bis(p-sulfonatophenyl)phenylphosphine (BSPP, 0.05uL, 55 mM), which chelates the remaining palladium ions. Each reaction was subsequently analyzed via inductively coupled plasma mass spectrometry (ICP-MS) to determine the amount of palladium incorporated into nanoparticles and thus the relative reduction rate of palladium ions under each set of growth conditions.

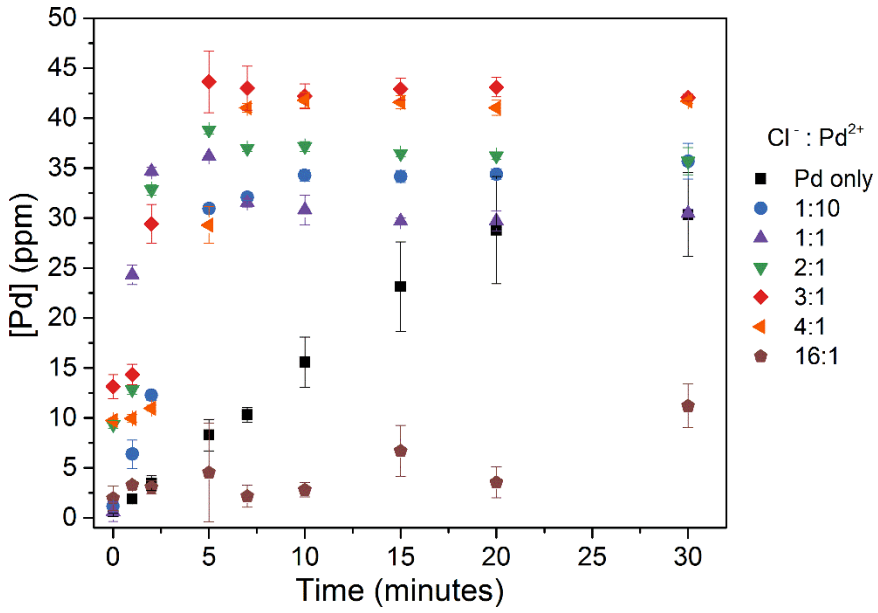

Figure 1. Graph of reduced palladium (palladium nanoparticle formation) over a thirty-minute reaction period with different chloride to palladium ion ratios.

Table 1. Effect of Added Chloride Ions on the Initial Rate of Palladium Ion Reduction

Cl^- : Pd^{2+}	Initial Rate of Pd^{2+} Reduction (ppm/min) [a]	Change in Rate (relative to Pd-only control) [b]
Pd Only	1.4	–
1:10	5.6	4.0 x
1:1	17.0	12.1 x
2:1	11.7	8.4 x
3:1	8.2	5.9 x
4:1	0.65	0.5 x
16:1	0.54	0.4 x

[a] Initial rate of Pd^{2+} reduction is calculated as the increase in the amount of palladium incorporated into nanoparticles from zero to two minutes of growth (slope of the data in Figure 1), as measured by ICP-MS.
[b] Ratio of the observed initial rate for a given condition to rate observed for the Pd-only control.

The addition of even a very low concentration of halide ions to the growth solution has a drastic effect on the reduction rate of palladium ions (Figure 1 and Figure S1). Indeed, with the introduction of one chloride ion for every ten palladium ions (49 μM chloride) there is a fourfold increase in the rate of palladium ion reduction in the first two minutes of the reaction as compared to the palladium-only control (Table 1). Further increases in the rate of reduction of palladium ions

can be seen upon increasing the ratio of chloride ions to palladium ions. A tenfold increase in the concentration of chloride ions in the growth solution—to a 1:1 chloride to palladium ratio—increases the rate of reduction of palladium ions so that it is approximately twelve times faster than the palladium-only control. Increasing the concentration of chloride ions above a 1:1 ratio of chloride to palladium begins a slowing trend in the average initial rate of palladium ion reduction (Figure 2). Once the ratio reaches four chloride ions for every one palladium ion, the reduction rate enhancing effect of the added chloride ions diminishes, and the initial rate of reduction is two times slower than the palladium-only control. Interestingly, the overall reduction rate is still considerably faster (Figures 1 and 2). Ultimately, for a more saturated system containing a 16:1 ratio of chloride to palladium, there is a distinct decrease in the rate of reduction of palladium ions to approximately three times slower than the rate of the control reaction and this slower rate is maintained throughout the course of the reaction (Figure 1). Notably, the oscillation of the amount of reduced palladium at early time points at this 16:1 ratio indicates cycles of etching and regrowth, which is expected in growth solutions containing high concentrations of chloride.[35] In the absence of chloride, the resulting particles are rough, pseudospherical, and are approximately 40 nm in diameter (Figure S2). With added chloride, the particles gradually become smoother and more faceted, with some particles developing into {111}-faceted shapes such as hexagonal plates, octahedra, truncated bitetrahedra, and icosahedra at 4:1 and 16:1 ratios of chloride to palladium (Figure S3). Overall, the shape and size distribution at these conditions is polydisperse, in part due to the seedless nature of the synthesis.

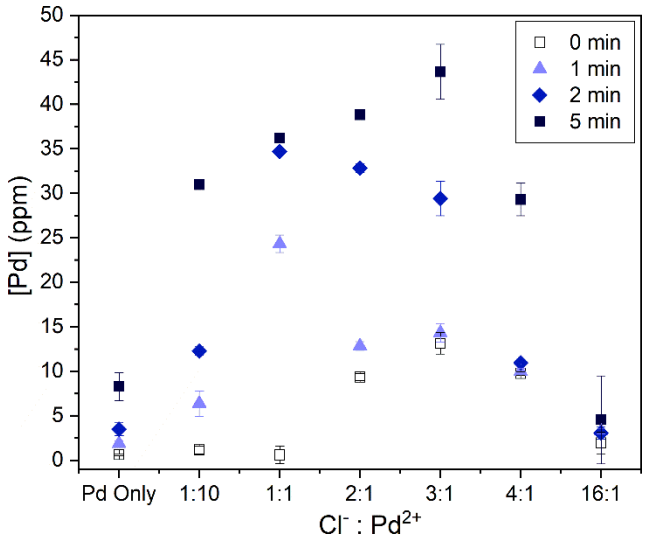

Figure 2. Comparative graph of the rates of palladium particle formation during the first five minutes of growth in the presence of chloride, as measured by ICP-MS.

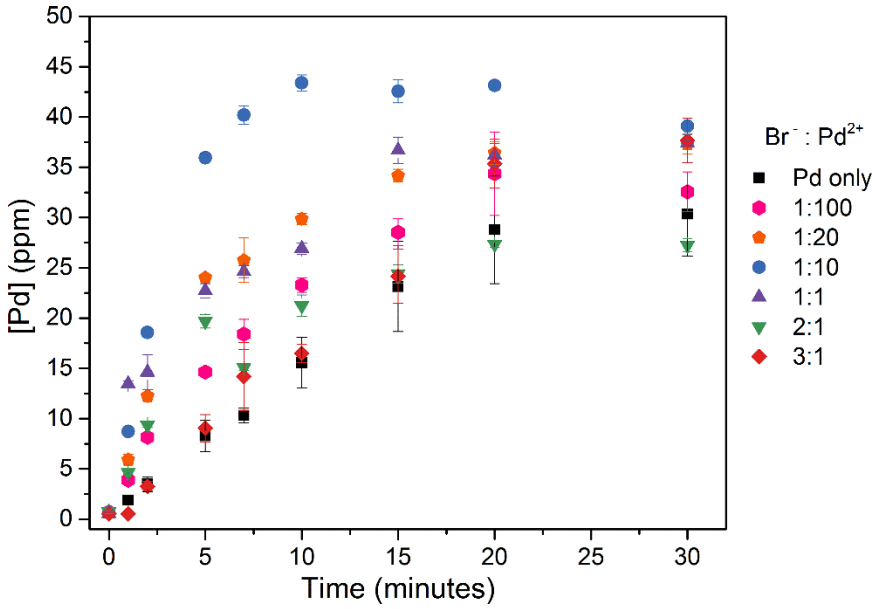

Figure 3. Graph of reduced palladium (palladium nanoparticle formation) over a thirty-minute reaction period with different bromide to palladium ion ratios.

Table 2. Effect of Added Bromide Ions on the Initial Rate of Palladium Ion Reduction

Br^- : Pd^{2+}	Initial Rate of Pd^{2+} Reduction (ppm/min) [a]	Change in Rate (relative to Pd-only control) [b]
Pd Only	1.4	–
1:100	3.7	1.9 x
1:20	5.8	4.1 x
1:10	9.0	6.4 x
1:1	7.0	5 x
2:1	4.3	3.1 x
3:1	1.4	–

[a] Initial rate of Pd^{2+} reduction is calculated as the increase in the amount of palladium incorporated into nanoparticles from zero to two minutes of growth (slope of the data in Figure 3), as measured by ICP-MS.
[b] Ratio of the observed initial rate for a given condition to rate observed for the Pd-only control.

As the size and binding affinity of the halide is increased, the trend remains the same while the concentrations required to increase the rate of reduction of palladium by a comparable amount are lower (Figure 3 and Figure S4). The addition of a single bromide ion for every one hundred palladium ions (4.7 μM bromide) doubles the initial rate of metal ion reduction relative to the palladium-only control (Table 2). Raising the bromide concentration to a 1:20 bromide to palladium ratio provides a fourfold increase in reduction rate relative to the control, which is comparable to what is observed for a 1:10 chloride to palladium ratio—twice the halide concentration. Likewise, the increased size of bromide as well as its greater binding affinity for palladium lead to an earlier leveling and decline in the reduction rate enhancement. As shown in Figure 4, a plot of the amount of reduced palladium at time points up to five minutes clearly illustrates that there is a significant decrease in the rate of metal ion reduction during these early time points once the ratio of palladium to bromide is greater than 1:1. At a ratio of 3:1 bromide to palladium, the initial rate of reduction is the same as the palladium-only control (Figure 4 and Figure S4). We note that this concentration of bromide is still less than the amount of bromide that would be present with the use of a bromide-based palladium precursor (such as $PdBr_4^{2-}$) and well

below the bromide associated with the use of cetyltrimethylammonium bromide or another bromide-containing surfactant. At the lowest ratio of bromide to palladium (1:100), the particles are rough and not well defined, but they quickly transition to small (~ 20 nm in diameter) stepped concave cubes and tripod-like bipyramids beginning at 1:20 bromide to palladium (Figure S5). Above a ratio of 2:1, the shape of the particles changes again, yielding larger, star-like nanorods as well as bipyramids.

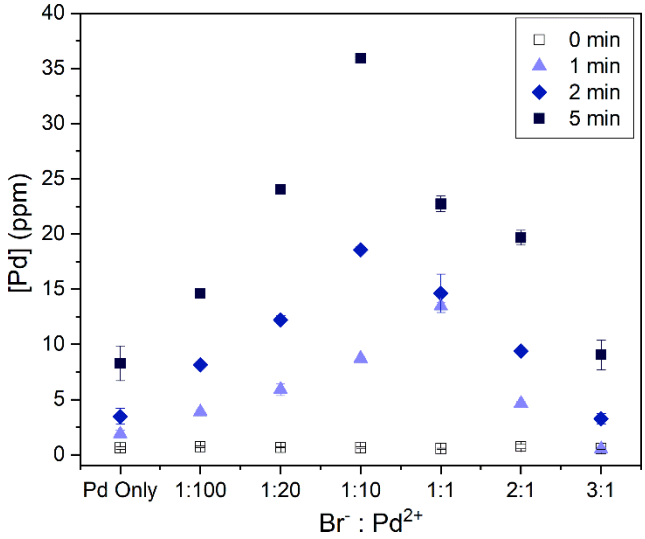

Figure 4. Comparative graph of the rates of palladium particle formation during the first five minutes of growth in the presence of bromide, as measured by ICP-MS.

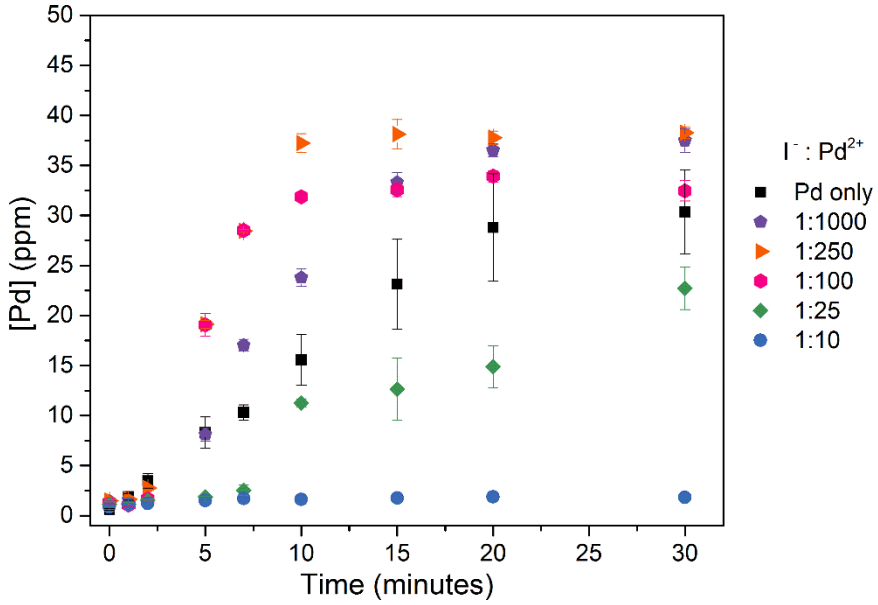

Figure 5. Graph of reduced palladium (palladium nanoparticle formation) over a thirty-minute reaction period with different iodide to palladium ion ratios.

The incorporation of iodide into the halide-free growth solution increases the overall rate of reaction when the iodide to palladium ratios are as low as 1:1000, 1:250, and 1:100. However, for these experiments the initial rate of reaction was calculated over the period from two minutes to seven minutes—rather than zero to two minutes—due to a brief induction period before the onset of significant particle growth when iodide is present (Figure 5 and Figure S6). The observed rate of reduction at an iodide to palladium ratio of 1:1000 is two times faster than the palladium-only control, similar to the rate increase at a bromide to palladium ratio of 1:100 (Table 3). At its maximum, the rate of reduction facilitated by iodide only reaches a four-fold increase before decreasing rapidly by seven-fold at a ratio of 1:25 and fourteen-fold at a ratio of 1:10. The particles generated at the enhanced rates of reduction are small (~16 nm) and pseudospherical, and no observable particles form at the 1:10 iodide to palladium ratio (Figure S7). The larger size and increased binding affinity of iodide lead to the onset of surface passivating effects at a much lower concentration than what is observed for chloride or bromide (Figure 6). Indeed, for the smaller

halides, a ratio of 1:10 halide to palladium yields a rate increase of approximately five and six times for chloride and bromide, respectively.

Table 3. Effect of Added Iodide Ions on the Initial Rate of Palladium Ion Reduction

I^- : Pd^{2+}	Initial Rate of Pd^{2+} Reduction (ppm/min) [a]	Change in Rate (relative to Pd-only control) [b]
Pd Only	1.4	–
1:1000	3.0	2.1 x
1:250	5.2	3.7 x
1:100	5.4	3.9 x
1:25	0.2	0.14 x
1:10	0.1	0.07 x

[a] Initial rate of Pd^{2+} reduction is calculated as the increase in the amount of palladium incorporated into nanoparticles from two to seven minutes of growth (slope of the data in Figure 5), as measured by ICP-MS.
[b] Ratio of the observed initial rate for a given condition to rate observed for the Pd-only control.

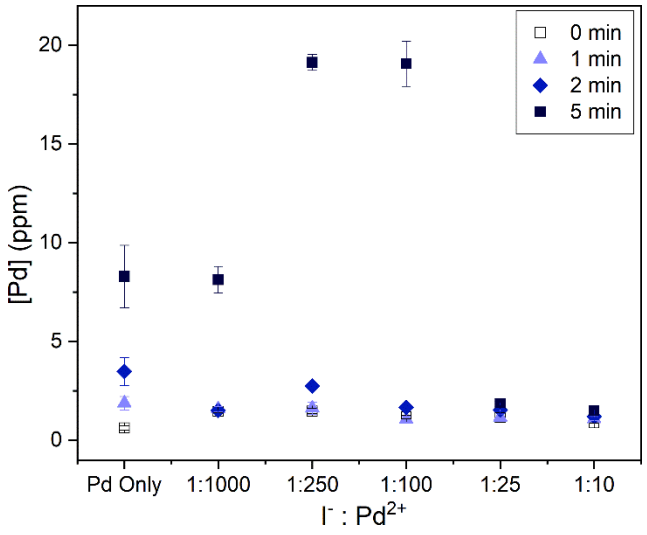

Figure 6. Comparative graph of the rates of palladium particle formation during the first five minutes of growth in the presence of iodide, as measured by ICP-MS.

This halide-free surfactant system provides a controlled platform for understanding the emergent effects of low concentrations of halides in solution-phase metal nanoparticle syntheses. Moreover, it provides a means of deconvoluting the individual influences of specific halides in systems with competitive interactions between multiple halide species, which are common in

nanoparticle synthesis. The data reported here show that, at micromolar concentrations, chloride, bromide, and iodide have a catalytic effect on the rate of reduction of palladium when there are no other competing halides. This increase in reduction rate is extremely sensitive both to the concentration of halide ions and to the nature of the halide present, and this low concentration effect on metal ion reduction rate differs substantially from the surface passivating and slowing effects commonly observed at even slightly higher (millimolar) concentrations. Bromide is known to have a higher binding affinity both for palladium ions and for the surface of a growing palladium nanoparticle than chloride does. Indeed, due to this stronger binding affinity of bromide, significantly less bromide is required to achieve a similar magnitude of kinetic enhancement. Conversely, the increased binding affinity of bromide, coupled with its larger ionic radius, leads to a transition to a surface passivating effect at a lower concentration than for chloride, which results in the slowing of reduction rate commonly reported in the particle growth literature. This trend is even more pronounced for iodide, where similar effects on reaction rate are observed with halide concentrations that are an order of magnitude lower than for bromide.

To explore whether this rate enhancing effect is primarily a surface effect or the result of palladium-halide complex formation in solution, palladium speciation was estimated for each of the chloride, bromide, and iodide conditions using Hyperquad Simulation and Speciation (HySS) software[31] along with reported formation constants for the respective halide complexes.[32, 33] For the growth conditions where the observed initial rate enhancement is approximately fourfold for each of the three halides, the most prevalent species in solution is the aqua complex, $[Pd(H_2O)_4]^{2+}$ (Tables S3-S5). At the halide concentrations required to reach this rate enhancement, 91%, 95%, and 99% of the palladium is predicted to exist as the aqua complex in the presence of chloride, bromide, and iodide, respectively. In each case, the only other predicted species is the complex

with a single halide ligand, $[PdX(H_2O)_3]^+$. In addition, for both bromide and iodide, a doubling of the palladium reduction rate is observed under conditions where the solution speciation is predicted to consist of ≥99% $[Pd(H_2O)_4]^{2+}$ (Tables S4 and S5). These estimates show that the formation of palladium-halide complexes in solution is not required for the reduction rate to be enhanced, suggesting that the trend observed from the collected experimental data is more likely to be the result of a surface interaction. In particular, the binding of halides to the growing nanoparticles can locally concentrate the halides at the nanoparticle surface, facilitating interactions with palladium ions.

In addition to following the order of increasing binding affinity of the halides for palladium, the observed trend of increasing effects on the rate of palladium reduction with increasing halide size and polarizability ($Cl^- < Br^- < I^-$) also mirrors what is commonly observed for oxidation-reduction reactions of inorganic coordination complexes that proceed via inner sphere bridged electron transfer processes. The collected data suggest that the incorporation of halides in low concentrations during nanoparticle growth facilitates the reduction of metal ions through a bridging ligand effect via an inner sphere electron transfer process, either by assisting the binding of the metal precursor to the particle surface with the appropriate configuration for electron transfer (Figure 7A) or by directly facilitating the electron transfer process itself (Figure 7B). Inner sphere electron transfer from a metal nanoparticle to an adsorbed metal ion is consistent with seed-mediated autocatalytic growth, and the sigmoidal shape of the palladium reduction curves indicates the involvement of an autocatalytic process. In contrast, upon saturation of the growing particle surface with adsorbed halide ions at higher halide concentrations, incoming palladium ions must displace the halides to access the surface or be reduced through an outer sphere electron transfer followed by metal atom adsorption (Figure 7C).

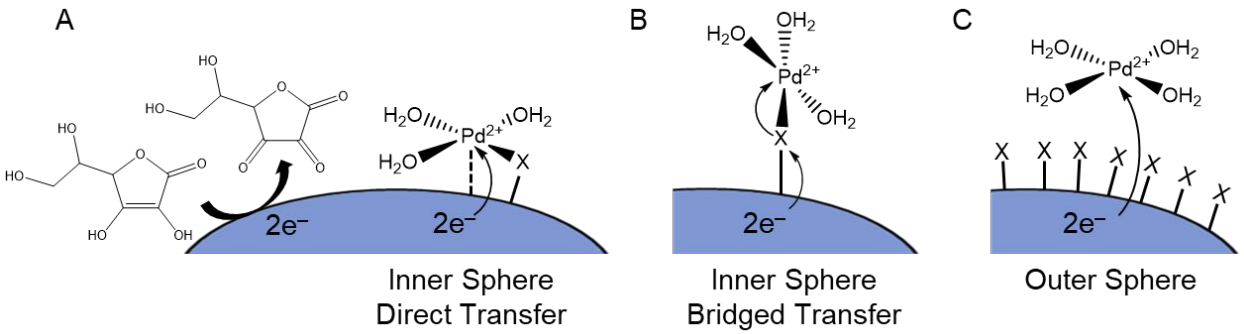

Figure 7. Schematic representation of possible electron transfer pathways. (A) Direct inner sphere electron transfer from the surface where the adsorption of the palladium complex is facilitated by coordination with a surface-bound halide. (B) Inner sphere electron transfer via a halide bridging ligand. (C) Outer sphere electron transfer, which is followed by halide displacement for metal atom adsorption.

A classic probe for inner sphere and outer sphere electron transfer mechanisms in homogeneous coordination chemistry is to test the rate of reduction in the presence of the pseudohalides anions azide (N_3^-) and thiocyanate (SCN^-). In those reactions, azide provides greater stabilization of the bridged intermediate during inner sphere electron transfer, and therefore a faster rate of reduction is expected with a bridging azide than with thiocyanate.[36] Both azide and thiocyanate ligands were tested for their ability to facilitate reduction of palladium ions in a halide-free surfactant. Interestingly, the incorporation of 1:1000, 1:100, or 1:10 azide to palladium slows the rate of metal ion reduction by four, five, and thirteen times, respectively, suggesting that the azide interaction with the surface is passivating even at extremely low concentrations (Table 4, Figures S8 and S9). The introduction of the thiocyanate ligand, however, yields rate enhancement effects similar to those of iodide (Table 4, Figures 8 and S10). The solution speciation of palladium in the presence of thiocyanate (Table S6) is also estimated to be the same as the speciation for iodide, with minimal formation of a palladium-thiocyanate complex under conditions of rate enhancement.[34] This observation suggests that the binding affinity of the introduced ligand to the palladium surface has a significant impact on its ability to facilitate metal ion reduction since sulfur

and iodide both bind strongly to the surface of noble metal nanoparticles. These results also indicate that surface-adsorbed halide ions are likely assisting in the binding of palladium complexes to the particle surface thereby facilitating direct electron transfer from the particle surface to the palladium ions (Figure 7A), rather than serving as a bridge for the electron transfer (Figure 7B). This experiment does not definitively rule out the possibility of a bridged electron transfer, since the binding strength and orientation of ligands influence heterogeneous electron transfer in a way that is not a strong factor in classic homogeneous coordination chemistry. For example, the distinct decrease in reduction rate when azide is present suggests that symmetric azide potentially binds to the surface in a parallel rather than perpendicular orientation, thus making it unable to facilitate either palladium ion adsorption or electron transfer. However, the slowed rate of metal ion reduction at higher concentrations—and therefore higher coverages—of halide ions is also inconsistent with an electron transfer to the metal ion through a halide ion bridge, since this mechanism of electron transfer should still be facile when the surface has a high coverage of halide ions.

Table 4. Effect of Added Pseudohalide Ions on the Initial Rate of Palladium Ion Reduction

X^-: Pd^{2+}	Initial Rate of Pd^{2+} Reduction with N_3^- (ppm/min) [a]	Change in Rate (relative to Pd-only control) [b]	Initial Rate of Pd^{2+} Reduction with SCN^- (ppm/min) [a]	Change in Rate (relative to Pd-only control) [b]
Pd Only	1.4	–	1.4	–
1:1000	0.32	0.23 x	1.5	1.1 x
1:100	0.26	0.19 x	3.9	2.8 x
1:10	0.11	0.08 x	0.16	0.11 x

[a] Initial rate of Pd^{2+} reduction is calculated as the increase in the amount of palladium incorporated into nanoparticles from two to seven minutes of growth (slope of the data in Figure 8), as measured by ICP-MS.
[b] Ratio of the observed initial rate for a given condition to rate observed for the Pd-only control.

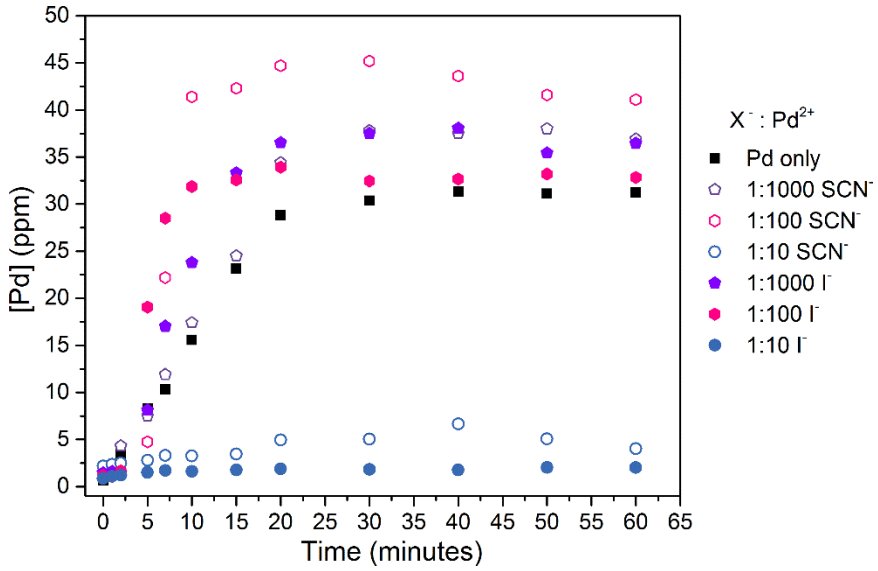

Figure 8. Comparison of the rate of formation of palladium particles in the presence of sodium iodide and sodium thiocyanate.

Importantly, while these detailed experiments conducted in a well-defined "halide-free" model system provide key insights into the mechanism and broad scope of halide-assisted metal ion reduction, the utility of this finely tunable reduction rate enhancement is not limited to CTA^+-HSO_4^- based growth systems. In our previous work on the development of shape-controlled palladium-copper bimetallic nanoparticles, we observed an eight-fold increase in the initial rate of palladium ion reduction with concentrations of iodide as low as 5 μM (an iodide to palladium ratio of 1:100) even in the presence of competing interactions from bromide ions in a 50 mM cetyltrimethylammonium bromide (CTAB) surfactant and chloride ions from the $PdCl_4^{2-}$ precursor.[30] When there are competitive surface interactions due to the presence of halide-based surfactants, it is possible that the iodide may additionally facilitate interaction of palladium ions with the particle surface by destabilizing a surface surfactant layer involving a less-strongly bound halide (here CTA^+ and bromide). Notably, the predicted speciation in this competitive system is 12% $[PdBr_3(H_2O)]^-$ and 88% $[PdBr_4]^{2-}$ with no expected formation of palladium-iodide complexes in solution. Post-synthetic detection of iodide at the surface of these particles via x-ray

photoelectron spectroscopy further corroborates a mechanism of halide-assisted reduction that takes place at the nanoparticle surface.[30] We originally hypothesized that this interaction was specific to iodide and that the iodide-triiodide redox couple might be assisting in the reduction of palladium at the nanoparticle surface due to its appropriate reduction potential relative to the reduction potential of the palladium ion precursor. However, the new results with bromide and chloride reported herein significantly expand the applicability of this halide-assisted metal ion reduction.

These new insights from the model system can also be applied to provide a more detailed understanding of previous reports involving the use of low concentrations of halides to modify particle shape in more common halide-based surfactants and with metals other than palladium. In particular, in the case of the silver-assisted synthesis of gold nanoparticles in cetyltrimethylammonium chloride (CTAC), the addition of micromolar concentrations of bromide and iodide had been observed to result in nanoparticles with higher coverages of silver at their surfaces, even if the amount of silver precursor in the growth solution was kept constant.[29] This was attributed to a destabilizing effect of the halides on the underpotentially-deposited silver layer, allowing the silver to diffuse to more stable sites and thereby enabling the deposition of more silver onto the surface without increasing the silver ion concentration in solution.[29] In addition, the authors observed an enhanced rate of gold ion reduction in this system with increasing bromide or iodide—still at low concentrations—however, they attributed this enhanced growth rate to the destabilization of the surface-passivating silver underpotential deposition layer, since bromide and iodide were generally known to slow gold ion reduction. The similarity of the reported behavior of this nanoparticle growth system to the halide-assisted metal ion reduction proposed in the current work provides an interesting opportunity to probe the effects of low concentrations of

bromide and iodide, separately, on the rates of reduction of gold and silver ions in the presence of competing high concentrations of chloride, primarily from the CTAC surfactant.

Indeed, measurements of the effect of bromide and iodide ions on the rates of gold and silver ion reduction in the silver-assisted synthesis of gold nanoparticles in 100 mM CTAC strongly support the hypothesis that halide-assisted metal ion reduction is directing particle growth in this bimetallic system as well. Importantly, the effect of bromide and iodide on the kinetics of silver ion reduction had not previously been probed. For a growth solution with 40 μL of 10 mM $AgNO_3$ and bromide to gold ratios of 1:20 (23 μM NaBr) and 1:10 (46 μM NaBr), there is an increase in the rate of gold ion reduction of ten and fifteen times, respectively, with the rate measured from ten to forty-five minutes (Figure S11A). Likewise, there is also a four-fold increase in the rate of silver ion reduction in the same system (bromide to silver ratios of 1:1.6 and 1:0.8) (Figure S11B). As expected, the resulting shape transition is from truncated ditetragonal prisms with no added bromide to concave cubes (Figure S12A-C).[29] When the volume of silver added to the growth solution is increased to 100 μL, enhancing effects of bromide on the rate of both gold and silver ion reduction are again observed (Figure S11C,D). The products remain concave cubes but become slightly more overgrown with increasing bromide (Figure S12D-F).

Iodide in this system has an interesting impact on the reduction rates of gold and silver ions. Indeed, when the ratio of iodide to gold in the presence of 40 μL of 10 mM silver is 1:200 (2.3 μM NaI) and 1:100 (4.6 μM NaI) the rate of gold ion reduction is four and five times faster, respectively (Figure S13A). In growth solutions containing 100 μL of silver, the impact of iodide on gold ion reduction is diminished and provides a marginal increase of 1.5 and 1.9 times faster for the same iodide to gold ratios of 1:200 and 1:100, respectively (Figure S13C). Conversely, iodide has a significant effect on silver ion reduction with 2.3 μM NaI and 4.6 μM NaI (iodide to

silver ratios of 1:16 and 1:8) yielding an increase in the rate of metal ion reduction by seven and nine times (Figure S13B). Further decreasing the ratio of iodide to silver to 1:40 and 1:20 by adding the same amounts of iodide to a growth solution with 100 μL of silver results in a rate increase of three and four times, respectively (Figure S13D). In both cases, the incorporation of iodide leads to the formation of stellated spheres (Figure S14). These results suggest that iodide has a more significant enhancing effect on the binding of silver ions to the surface than it does for gold. This is potentially due to the lack of halide ligands on the silver ion precursor ($AgNO_3$). We have previously observed a more significant effect of iodide on the rate of palladium ion reduction relative to gold ion reduction in a system containing both metal ions.[19] Both metal precursors in that case were chloride salts, however, palladium complexes are known to undergo significant hydrolysis, replacing halide ligands with water ligands, which have a weaker binding affinity for the nanoparticle surface. Additionally, a similar magnitude of change in reduction rate will also result in a greater fold increase in reduction rate for the ion that is already reduced more slowly—silver in the case of silver-assisted gold nanoparticle syntheses.

Conclusions

The collective data provide evidence for a halide-assisted metal ion reduction mechanism in the presence of micromolar concentrations of halides in both a "halide-free" platform and in bimetallic systems containing competing halides from surfactants and metal precursors. Further, the catalytic effects of halides on the rate of metal ion reduction combined with results from experiments with pseudohalide ions suggest that the incorporated halide facilitates inner sphere electron transfer from the nanoparticle surface to a bound metal ion. We propose a mechanism for this assisted electron transfer which involves a coordination effect whereby adsorbed halides provide an anchor for the incoming metal complex to bind to the surface in the correct geometry

and with sufficient affinity, thus facilitating direct electron transfer from the growing particle surface. While the shapes of the monometallic palladium nanoparticles that result from the fundamental experiments conducted in CTA^+-HSO_4^- are somewhat polydisperse, these model experiments show that micromolar concentrations of halide ions have a catalytic and shape-influencing effect on nanoparticle growth that is disproportionate to their low concentration. We demonstrate that this rate-enhancing effect is not limited to iodide ions, but can be extended to chloride, bromide, and the pseudohalide thiocyanate as well, which provides new handles for tuning nanoparticle formation. The "halide-free" model system highlights fundamental behavior and the broad scope of this phenomenon, while the application of halide-assisted metal ion reduction to more complex growth solutions showcases its utility in shape and composition control.

Importantly, we have shown that this halide-assisted metal ion reduction is a versatile tool to enable differential control of metal ion reduction rates, and thereby shape control, in one-pot co-reduction syntheses where the relative binding affinity of the incorporated halide to different metal precursors can yield dissimilar effects on different metal ions. This includes combinations such as gold/silver, gold/palladium, and palladium/copper, and the relative universality of metal-halide interactions opens possibilities for numerous other pairs. The ability to differentially control the reduction rate of two species is particularly important in situations where one metal precursor is more difficult to reduce, but where simply increasing the overall reduction rate of all metal ions using approaches such as raising the pH or increasing the temperature results in compositional segregation and/or deterioration of shape. The halide-assisted reduction approach is feasible in syntheses spanning a range of standard methodologies that includes halide-based surfactants (CTAB and CTAC) at concentrations up to 100 mM as well as seed-mediated syntheses.

Additionally, the mechanism proposed herein provides further insight into potential influences of trace impurities, which are known to cause issues with reproducibility in nanoparticle synthesis. By adding controlled micromolar concentrations of halide ions to a growth solution, it may be possible to troubleshoot irreproducibility between laboratories or chemical batches by subtly tuning reaction rate without affecting surface passivating interactions. Consequently, halide-assisted metal ion reduction provides a route to increasingly well-designed particle syntheses with deliberately controlled compositions and morphologies under mild aqueous phase reaction conditions.

Conflicts of Interest

There are no conflicts of interest to declare.

Acknowledgements

Acknowledgement is made to the donors of The American Chemical Society Petroleum Research Fund for partial support of this research. This work was also supported by start-up funding from Wesleyan University. The authors thank Prof. T. David Westmoreland (Wesleyan University) for helpful discussions. ICP-MS measurements were performed at the Yale Analytical and Stable Isotope Center (YASIC), a Yale Institute for Biospheric Studies (YIBS) research center. SEM imaging at Wesleyan University was supported by the National Science Foundation Major Research Instrumentation program under Grant No. 1725491. TEM imaging and additional SEM characterization was carried out at Yale University at The Yale Institute for Nanoscience and Quantum Engineering (YINQE).

Notes and References

1. D. D. Robertson and M. L. Personick, *Chem. Mater.*, 2019, **31**, 1121-1141.
2. Q. Jin, Y. Deng, X. Chen and J. Ji, *ACS Nano*, 2019, **13**, 954-977.
3. J.-E. Park, Y. Jung, M. Kim and J.-M. Nam, *ACS Cent. Sci.*, 2018, **4**, 1303-1314.
4. Q. Zhang and H. Wang, *ACS Catal.*, 2014, **4**, 4027-4033.
5. K. An and G. A. Somorjai, *ChemCatChem*, 2012, **4**, 1512-1524.
6. B. Roldan Cuenya and F. Behafarid, *Surf. Sci. Rep.*, 2015, **70**, 135-187.
7. S. Alayoglu, A. U. Nilekar, M. Mavrikakis and B. Eichhorn, *Nat. Mater.*, 2008, **7**, 333.
8. D. D. Robertson, M. E. King and M. L. Personick, *Top. Catal.*, 2018, **61**, 348-356.
9. J. R. Kitchin, J. K. Nørskov, M. A. Barteau and J. G. Chen, *Phys. Rev. Lett.*, 2004, **93**, 156801.
10. B. W. Goodfellow, Y. Yu, C. A. Bosoy, D.-M. Smilgies and B. A. Korgel, *J. Phys. Chem. Lett.*, 2015, **6**, 2406-2412.
11. R. J. Macfarlane, M. N. O'Brien, S. H. Petrosko and C. A. Mirkin, *Angew. Chem. Int. Ed.*, 2013, **52**, 5688-5698.
12. K. D. Gilroy, A. Ruditskiy, H.-C. Peng, D. Qin and Y. Xia, *Chem. Rev.*, 2016, **116**, 10414-10472.
13. H. Jung, M. E. King and M. L. Personick, *Curr. Opin. Colloid Interface Sci.*, 2019, **40**, 104-117.
14. M. L. Personick and C. A. Mirkin, *J. Am. Chem. Soc.*, 2013, **135**, 18238-18247.
15. X. Ye, C. Zheng, J. Chen, Y. Gao and C. B. Murray, *Nano Lett.*, 2013, **13**, 765-771.
16. D. K. Smith, N. R. Miller and B. A. Korgel, *Langmuir*, 2009, **25**, 9518-9524.
17. J. E. Millstone, W. Wei, M. R. Jones, H. Yoo and C. A. Mirkin, *Nano Lett.*, 2008, **8**, 2526-2529.
18. S. E. Lohse, N. D. Burrows, L. Scarabelli, L. M. Liz-Marzán and C. J. Murphy, *Chem. Mater.*, 2014, **26**, 34-43.
19. M. E. King and M. L. Personick, *Part. Part. Syst. Char.*, 2017, **34**, 1600422.
20. S. Ghosh and L. Manna, *Chem. Rev.*, 2018, **118**, 7804-7864.
21. A. L. Stone, M. E. King, S. P. McDarby, D. D. Robertson and M. L. Personick, *Part. Part. Syst. Char.*, 2018, **35**, 1700401.
22. M. M. Bower, C. J. DeSantis and S. E. Skrabalak, *J Phys Chem C.*, 2014, **118**, 18762-18770.
23. J. Zhang, M. R. Langille, M. L. Personick, K. Zhang, S. Li and C. A. Mirkin, *J. Am. Chem. Soc.*, 2010, **132**, 14012-14014.
24. T. Ming, W. Feng, Q. Tang, F. Wang, L. Sun, J. Wang and C. Yan, *J. Am. Chem. Soc.*, 2009, **131**, 16350-16351.
25. T. K. Sau and C. J. Murphy, *J. Am. Chem. Soc.*, 2004, **126**, 8648-8649.
26. H.-Y. Ahn, H.-E. Lee, K. Jin and K. T. Nam, *J. Mater. Chem. C*, 2013, **1**, 6861-6868.
27. W. Niu, S. Zheng, D. Wang, X. Liu, H. Li, S. Han, J. Chen, Z. Tang and G. Xu, *J. Am. Chem. Soc.*, 2009, **131**, 697-703.
28. H.-L. Wu, C.-H. Kuo and M. H. Huang, *Langmuir*, 2010, **26**, 12307-12313.
29. M. R. Langille, M. L. Personick, J. Zhang and C. A. Mirkin, *J. Am. Chem. Soc.*, 2012, **134**, 14542-14554.
30. M. E. King and M. L. Personick, *J. Mater. Chem. A*, 2018, **6**, 22179-22188.

31. L. Alderighi, P. Gans, A. Ienco, D. Peters, A. Sabatini and A. Vacca, *Coord. Chem. Rev.*, 1999, **184**, 311-318.
32. L. I. Elding and L.-F. Olsson, *Inorg. Chim. Acta*, 1986, **117**, 9-16.
33. C. J. Le Roux and R. J. Kriek, *Hydrometallurgy*, 2017, **169**, 447-455.
34. C. J. Le Roux, P. Gans and R. J. Kriek, *J. Coord. Chem.*, 2014, **67**, 1520-1529.
35. H. Zhang, M. Jin, Y. Xiong, B. Lim and Y. Xia, *Acc. Chem. Res.*, 2013, **46**, 1783-1794.
36. S. W. Barr and M. J. Weaver, *Inorg. Chem.*, 1984, **23**, 1657-1663.

Table of Contents Graphic

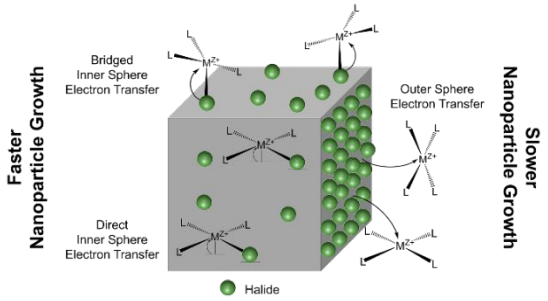

Halide ions catalytically enhance metal ion reduction rate, providing a versatile design tool for controlling metal nanoparticle growth.